AIAA JOURNAL
Vol. 42, No. 7, July 2004

Adjustment of Subgrid-Scale Parameterizations to Strong Streamline Curvature

Frank Holzäpfel*
DLR, German Aerospace Research Center, Oberpfaffenhofen, 82234 Wessling, Germany

A subgrid-scale model correction for large eddy simulations that address flowfields with embedded areas of poorly resolved strong streamline curvature effects is proposed. The devised modification is termed NaCoo and provides an isotropic correction of the subgrid-scale viscosity based on local centrifugal stability. The degree of stability is identified via a rotational Richardson number that is determined based on non-Galilean-invariant streamline curvature at every grid point. NaCoo allows for a more realistic representation of inadequately resolved coherent turbulent vortices. Its main benefits are 1) conservation of the peak vorticity in the vortex cores, 2) reduction of vortex core radius growth rates, 3) an approach to properties of tangential velocity profiles found in experiments 4) allowance for appropriate turbulence levels in the vicinity of the vortices, and 5) non suppression of vortex core meandering. The derivation of NaCoo, its properties, and sensitivity to numerical and vortex parameters are described in detail. Applications of the correction to single vortices and aircraft wake vortices in a quiescent and turbulent environment demonstrate the capabilities of the pragmatic correction.

Nomenclature

a	=	acceleration
b	=	vortex spacing
C	=	constant
c_S	=	model coefficient
D	=	magnitude of deformation tensor, $D_{ij} = 2S_{ij}$
e	=	unit vector
F_r	=	restoring force
p	=	dynamic pressure fluctuation
Ri	=	Richardson number
r	=	radial coordinate
r_c	=	vortex core radius
S_{ij}	=	strain rate tensor
t	=	time
u	=	axial velocity
v	=	(lateral) velocity
w	=	vertical velocity
x	=	axial coordinate
y	=	lateral coordinate
z	=	vertical coordinate
α	=	model coefficient
Γ	=	circulation
Δ	=	effective mesh size
ν	=	kinematic viscosity
ρ	=	density
τ_{ij}	=	subgrid-scale (SGS) fluxes of momentum
Ω	=	magnitude of vorticity
ω	=	oscillation frequency

Subscripts

n	=	normal direction
SGS	=	subgrid scale
t	=	tangential direction
θ	=	azimuthal direction
0	=	initial value

Superscripts

$*$	=	normalized quantity, based on b_0, Γ_0
$'$	=	normalized quantity, based on Δ, r_{c0}, Γ_0
$''$	=	SGS fluctuation

Received 27 October 2003; revision received 25 February 2004; accepted for publication 26 February 2004.

*Research Scientist, Institute of Atmospheric Physics; frank.holzaepfel@dlr.de.

I. Introduction

A SEEMINGLY endless number of efforts have been geared toward the achievement of approaches for adequate numerical treatment of turbulent flows with pronounced streamline curvature and rotation effects. An impressive amount of semi-empirical modifications for curvature effects were developed for the class of Reynolds-Averaged Navier–Stokes approaches, in particular, for the widespread, cost-efficient, and robust k–ϵ turbulence model.[1] Until today, numerous corrections had been suggested for eddy-viscosity models,[2] during which time it was generally recognized that the more costly second-moment turbulence closures have a fundamental advantage over eddy-viscosity models due to the explicit appearance of rotation and curvature terms in the transport equations.[3,4] The even more costly large-eddy simulation (LES) explicitly simulates the Navier–Stokes equations and, thus, fully considers the effects of curvature and rotation in the resolved scales. Therefore, LES have been applied to improve the fundamental understanding of the effects of rotating flows.[5] Driven by the ever-growing computational power, LES is also increasingly used for applied problems.[6,7] However, such applications often demand an unpleasant tradeoff between the complexity of the tackled problem and an adequate numerical representation such that the impact of the subgrid-scale (SGS) closure may become more dominant. Another more specific way to circumvent resolution requirements is the vorticity confinement method,[8] which preserves tight vortices even in coarse numerical meshes. Recent developments of this method try to counterbalance vorticity confinement and numerical diffusion.[9] This could allow researchers to address problems where vortex decay is of relevance.

LES explicitly simulate turbulent eddies that are resolved on a computational grid, whereas smaller-scale fluctuations are smoothed and modeled by SGS closures. If the scales of eddies that dominate turbulent transport are resolved, the subgrid model primarily has to provide an appropriate energy sink that prevents a tailback of small-scale energy. If, however, the larger-scale turbulence is suppressed by stabilizing body forces, such as the buoyancy force in a stably stratified environment or centrifugal forces in a rotating flow, or is damped in the vicinity of a wall, the SGS model may locally control turbulent transport. As a consequence, the flow regions that are strongly affected by body forces may represent a

solution of the SGS model rather than of the Navier–Stokes equations. Even without strong damping of the resolved turbulence, the velocity gradients of poorly resolved embedded areas of strong coherent rotation may dominate turbulent fluctuations. As a consequence, simulation results may be adulterated because, in general, the effects of centrifugal and Coriolis forces are not represented by the SGS closure.

These effects become most objectionable when an appropriate resolution of all involved length scales is not feasible. An example is given by simulations that investigate the interaction of aircraft wake vortices with environmental conditions, which basically suffer from limited resolution. This becomes immediatly clear for an LES of wake vortex evolution in a convectively driven atmospheric boundary layer.[10] Ideally, the LES should resolve length scales spanning the order of approximately 0.1 m in the strongly rotating vortex cores to the order of 1000 m in the atmosphere, where the latter length scale roughly corresponds to the inversion height of a convective boundary layer. An appropriate equidistant numerical mesh would need $\mathcal{O}(10^{12})$ mesh points, whereas current grids are limited to about 10^7–10^9 meshes. There are many other applications where it is desirable to model flows with strong streamline curvature with a modest number of grid points and without the need to resolve all details of the flow. An example for a geophysical flow is the simulation of tornadoes, technical applications that comprise the flow around aircraft wings in high-lift configuration, fighter aircraft under high angles of attack, or swirl combuster-type flows. In the latter example, the simulation of chemical reactions may dominate the numerical effort and an adequate representation of the swirling flowfield must be realized based on a relatively coarse grid.

The dynamic SGS model,[11] which is widespread for lower Reynolds number applications, suppresses successfully the SGS viscosity in a poorly resolved rectilinear vortex, provided that the direction employed for the averaging of SGS model coefficients coincides with the axis of rotation. However, in a test of the dynamic model, we already found that for small angles of less than 5 deg between the axis of rotation and the averaging direction, spurious SGS viscosity patches develop in the vortex core region that distort the vortex and cause numerical instability. The complex deformations that wake vortex pairs experience during their evolution prevent the determination of directions of statistical homogeneity that would allow for adequate averaging. A possible alternative is the Lagrangian dynamic model,[12] which accumulates averages along streamlines, a procedure that, however, is not Galilean-invariant.

The suggested SGS model modification termed NaCoo provides an isotropic correction of the SGS viscosity based on the degree of local centrifugal stability. The stability is identified via a rotational Richardson number that is determined based on streamline curvature at every grid point. The name NaCoo refers to the procedure that determines the curvature radius in natural coordinates. NaCoo was already partially introduced in Ref. 13. The title of this paper employs the objective "Strong" to characterize the degree of streamline curvature that increases when the center of a vortex is approached where the curvature eventually tends to infinity, whereas the curvature radius inversely goes to zero. Because of its low additional computational expense, NaCoo is suitable for LES approaches that follow the efficient philosophy of investment of as much as possible of the available computational resources in an outmost resolution of the grid scale flow and to consume as little as possible for sophisticated SGS closures and numerical schemes. The approach can, in principle, be adapted to any eddy-viscosity closure model. In contrast to the dynamic SGS model, which requires averaging of SGS model coefficients to stabilize the solution, the current approach is calculated locally at every grid point and, thus, may resolve even the smallest embedded vortices.

Because the correction is sensitive to streamline curvature, it is not Galilean-invariant. However, for many practical applications, including aircraft wake vortices, this is not a severe shortcoming because streamline curvature is determined naturally in an inertial frame of reference. A Galilean-invariant criterion for curvature and rotation can be defined when the direction of the principal axes of the strain rate tensor[14] is tracked. The higher complexity and increased numerical effort (20% plus vs our approach with a 5% penalty) of this alternative to streamline curvature[14] may counterbalance the advantage of Galilei invariance, at least for the large number of cases where Galilei invariance is of no relevance. Further SGS model modifications for streamline curvature effects are described in Refs. 15 and 16.

After a brief introduction of the applied basic equations and numerical methods appears in Sec. II, and the effects of the Smagorinsky closure on a single vortex are discussed in Sec. III. In Sec. IV, the stabilizing and destabilizing effects of streamline curvature are reviewed, and in Sec. V, the SGS correction NaCoo is introduced and compared to Proctor's approach.[13] Furthermore, aspects of the Galilei invariance issue are assessed. Section VI describes applications of NaCoo to single vortices and to aircraft wake vortices in a quiescent and turbulent environment. Finally, the sensitivity of the correction on numerical and vortex parameters is discussed in Sec. VII.

Beyond the applications shown in this paper, NaCoo has been applied to simulations of aircraft-generated multiple vortex systems that are expected to trigger cooperative instability mechanisms that lead to a premature onset of decay.[17] Another application of NaCoo addresses the reproduction of turbulence levels measured in wake vortices at different distances behind the generating aircraft (personal communication with R. E. Robins in 2003).

II. Governing Equations

To provide the background for the discussion of the streamline curvature correction, the basic equations and numerical methods of the applied code LESTUF[18] are briefly introduced. LESTUF was originally developed for studies of stratified, sheared, and homogeneous turbulence. In space and time the code solves the mass conservation equation

$$\frac{\partial u_i}{\partial x_i} = 0 \tag{1}$$

and the Navier–Stokes equations for the resolved velocity vector

$$\frac{\partial u_i}{\partial t} + \frac{\partial}{\partial x_j} u_i u_j = -\frac{1}{\rho}\frac{\partial p}{\partial x_i} - \frac{\partial \tau_{ij}}{\partial x_j} \tag{2}$$

in an unsteady, incompressible, and three-dimensional fluid flow. In Eq. (2), friction is represented by the SGS fluxes of momentum that result from the nonlinear term in Eq. (2) after filtering on the mesh scale. They are parameterized following an ansatz by Deardorff[19]:

$$\tau_{ij} := \overline{u_i'' u_j''} - \tfrac{1}{3}\overline{u_i'' u_i''}\delta_{ij} = -2\nu_{\mathrm{SGS}} S_{ij} \tag{3}$$

with the strain rate tensor

$$S_{ij} = \frac{1}{2}\left(\frac{\partial u_i}{\partial x_j} + \frac{\partial u_j}{\partial x_i}\right) \tag{4}$$

The SGS viscosity is modeled by Smagorinsky's approach[20]:

$$\nu_{\mathrm{SGS}} = (c_S \Delta)^2 (2 S_{ij} S_{ji})^{\frac{1}{2}} \tag{5}$$

where the constant $c_S = 0.165$ is set to the theoretical value for isotropic turbulence.

The physical fields are discretized on a Cartesian staggered grid and integrated in space and time by second-order finite differencing. Time advancement is performed by a prognostic step for advection and diffusion by the use of the second-order Adams–Bashforth scheme, followed by a diagnostic step that solves the Poisson equation for the dynamic pressure. The integration scheme is nondissipative and only weakly dispersive. The computational grid is equidistant, and periodic boundary conditions are employed in all directions. For anisotropic numerical meshes, the effective mesh size is calculated according to the fitting formula of Scotti et al.[21]

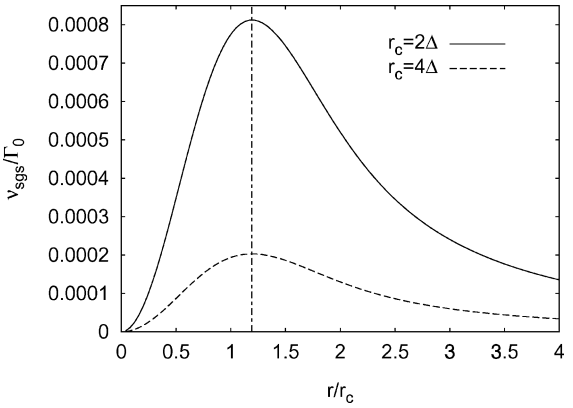

Fig. 1 Radial profiles of normalized SGS viscosity for Smagorinsky closure and two different numerical resolutions.

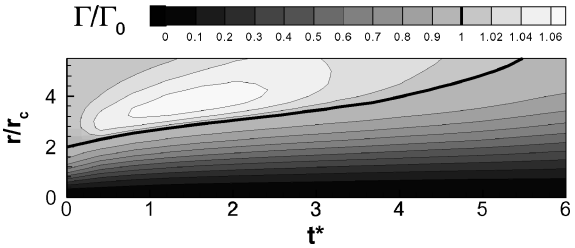

Fig. 2 Temporal evolution of radial circulation distribution of a turbulent wake vortex in quiescent environment.

III. Effects of the Smagorinsky Approach

To illustrate the effects of strong streamline curvature, the Lamb–Oseen vortex is employed as a generic vortex. Any other analytically given continuously differentiable vortex profile could have been used. The tangential velocity profile of the Lamb–Oseen vortex consists of rigid-body rotation close to its center and a smooth blend to the potential vortex on large radii according to

$$v_\theta(r) = (\Gamma_0/2\pi r)\left[1 - \exp\left(-1.257r^2/r_c^2\right)\right] \tag{6}$$

As baseline case, a vortex with a core radius of $r_{c0} = 4$ m and a circulation of $\Gamma_0 = 565\ \mathrm{m}^2/\mathrm{s}$ is employed. To represent wake vortices generated by a B-747 aircraft, two counter-rotating vortices with a vortex spacing of $b_0 = 47$ m are superposed. For wake vortices, time is normalized by the time scale $2\pi b_0^2/\Gamma_0$.

To illustrate the impact of the Smagorinsky closure on coherent vortices, the Smagorinsky eddy viscosity [Eq. (5)] normalized by Γ_0 is derived for the Lamb–Oseen vortex:

$$\nu_{SGS}(r)/\Gamma_0 = \left[(c_S\Delta)^2/\pi r_c^2\right] \times \left[r_c^2/r^2 - \left(1.257 + r_c^2/r^2\right)\exp\left(-1.257r^2/r_c^2\right)\right] \tag{7}$$

and plotted in Fig. 1 for different vortex core resolutions. In Eq. (5), the strain rate tensor is applied for convenience in curvilinear coordinates, because then only the radial-tangential component of the strain rate tensor, $(r/2)[(\partial v_\theta/r)/\partial r]$, contributes to ν_{SGS}.

Note that in Eq. (7) the resolution of the vortex core, (Δ/r_c), enters to the power of two. Therefore, in poorly resolved vortex cores enhanced values of SGS viscosity are generated (Fig. 1) that cause large vortex core growth rates and a strong reduction of peak vorticity. Figure 1 delineates that ν_{SGS} increases from zero at $r = 0$ (rigid-body rotation) to a maximum at $1.19r_c$ and then decreases again. (Obviously, when $r = 0$ is approached, molecular diffusion becomes relevant. Because this is a singular situation, molecular diffusion can be neglected in the LES.) As a consequence, the radial velocity profiles deviate from the family of self-similar Lamb–Oseen vortex profiles that develop for laminar simulations with constant viscosity. This is shown in Fig. 2, which shows the temporal evolution of the radial circulation distribution of a turbulent wake vortex in a quiescent environment. At $t^* = 0$, the initialized Lamb–Oseen vortex attains the maximum circulation of one at about $r > 2r_{c0}$. Later on, an overshoot of circulation is produced that reaches a maximum of 7% at around $t^* = 1.5$.

In this simulation, aircraft-induced turbulence was taken into account by the initial addition of a three-dimensional random perturbation field to the swirling flow, such that the perturbations reach maximum rms values of 2 m/s at the core radius and decay exponentially for smaller and larger radii. This type of turbulence initialization is referred to as case b. In Sec. VI, another scenario termed case a is considered: In addition to the aircraft-induced turbulence, weak to moderate, anisotropic, and decaying atmospheric turbulence is superimposed on the whole velocity field. The atmospheric turbulence obeys prescribed spectra with rms velocities of 0.38 m/s in the horizontal and 0.21 m/s in the vertical direction. The length scales of the most energetic eddies amount to 60–90 m. The turbulence initializations of both cases are described in detail in Ref. 22.

IV. Centrifugal Stability

Although the concept of centrifugal stability is well known from the literature,[23] it is briefly introduced here for an easier understanding of the following sections. Figure 3 and Eq. (8) illustrate that a fluid element in a vortex flow that is radially displaced by dr and retains its angular momentum ($v_\theta r = \text{const}$) experiences a restoring force. The restoring force is proportional to the difference between the centripetal forces acting on the displaced fluid element and its environment; that is, it is proportional to the difference between the velocity of the fluid element squared and the velocity of the surrounding mean vortical flow squared and inversely proportional to the local curvature radius:

$$F_r = -\rho\left[\frac{v_{\theta,r+dr}^2}{r+dr} - \frac{\hat{v}_\theta^2}{r+dr}\right], \qquad \hat{v}_\theta = \frac{v_\theta r}{r+dr} \tag{8}$$

By means of a Taylor series expansion and with higher-order terms neglected, F_r can be expressed differentially:

$$F_r \approx -\frac{1}{r^3}\frac{\partial}{\partial r}\left[\rho(v_\theta r)^2\right]dr \tag{9}$$

Equating the restoring force to the inertia of the fluid element yields a differential equation that describes undamped oscillations of the displaced fluid element:

$$\frac{\partial^2 r}{\partial t^2} + \underbrace{\frac{1}{r^3}\frac{\partial}{\partial r}\left[(v_\theta r)^2\right]}_{\omega^2} r = 0 \tag{10}$$

The restoring force, the oscillation frequency, and, hence, the vortex stability achieve maximum values at the vortex center and vanish at about $2r_c$ where the vortex attains constant circulation (cf. Fig. 3).

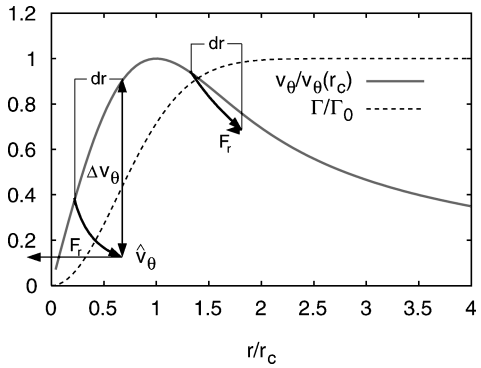

Fig. 3 Schematic of the restoring force experienced by a radially displaced fluid element in a Lamb–Oseen vortex and respective circulation profile.

For negative gradients of $v_\theta r$, the oscillation frequency becomes imaginary and the vortex becomes unstable. Unstable flow conditions may occur, for example, at the edges of a swirling jet where they cause enhanced mixing or in the boundary-layer flow along a concave wall where instability may lead to the formation of Görtler vortices.

V. SGS Model Correction

A. Richardson Number

The following considerations are based on the Richardson number for streamline curvature effects that Bradshaw[24] derived in analogy to the gradient Richardson number for buoyancy effects in stably stratified flows. Bradshaw's Richardson number

$$Ri = \frac{2v}{r^2}\frac{\partial vr}{\partial r}\Bigg/\left(\frac{\partial v}{\partial r}\right)^2 \tag{11}$$

relates the oscillation frequency squared of the radially displaced fluid element [ω^2 in Eq. (10)] to the square of a "typical frequency scale of the shear flow." However, the choice of the latter frequency scale is misleading. For example, in an axisymmetric vortex, $\partial v/\partial r$ vanishes at the core radius. As a consequence, the Richardson number would go to infinity at $r = r_c$, where erroneously maximum stability would be assumed as it was in Ref. 25. (Recently, the flaw in Ref. 25 was revised.[26]) As shown in the preceding section, however, maximum stability is attained in the center of the vortex. A consistent formulation is achieved when the deformation tensor squared is employed in the denominator instead. In curvilinear coordinates, chosen for convenience, this corresponds to

$$Ri = \frac{2v_\theta}{r^2}\frac{\partial v_\theta r}{\partial r}\Bigg/2\left(r\frac{\partial v_\theta/r}{\partial r}\right)^2 \tag{12}$$

Radial profiles of the components of Eq. (12) are plotted for the Lamb–Oseen vortex in Fig. 4. The oscillation frequency in the numerator normalized by $(\pi r_c^2/\Gamma_0)^2$ inceases from zero at $r/r_c > 2$ to its maximum of $\pi/2$ at the vortex center. The normalized deformation tensor in the denominator has a maximum at $r_c = 1.19$, attains the same value as the oscillation frequency at the core radius, goes to zero at the vortex center and to low values on large radii. Consequently, the Richardson number increases monotonically from zero at $r/r_c > 2$, reaches a value of 1 at $r = r_c$, and goes to infinity when approaching $r = 0$.

Shen et al.[15] extended the Richardson number formulation to three dimensions:

$$Ri = \Omega^2/D^2 + \Omega/D \tag{13}$$

Because Eq. (13) cannot discriminate between vorticity of a plane shear flow and vorticity of coherent rotation, an additional discriminator algorithm has to be applied.

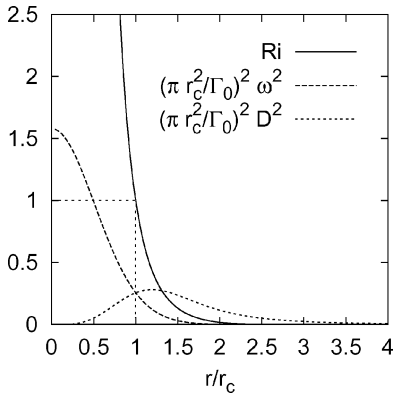

Fig. 4 Radial profiles of Richardson number, normalized oscillation frequency squared, and normalized deformation tensor squared for a Lamb–Oseen vortex.

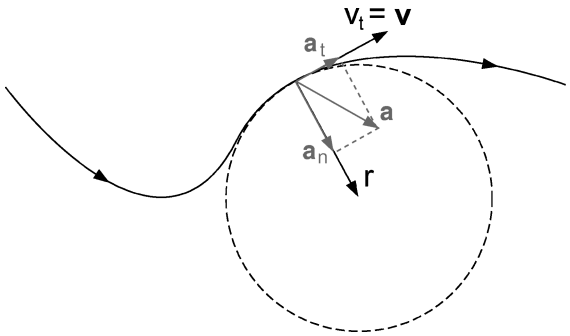

Fig. 5 Determination of the tangential velocity v_t and the curvature radius r in natural coordinates.

We apply instead the modified ansatz by Bradshaw [Eq. (12)] in natural coordinates:

$$Ri = \frac{2v_t}{r}\left(\frac{v_t}{r} + \frac{\partial v_t}{\partial r}\right)\Bigg/D^2 \tag{14}$$

that does not require a discriminator function. It employs the tangential velocity directly along a local streamline whose curvature is given by an inscribed circle with radius r (Fig. 5). For an undisturbed axisymmetric vortex, both Richardson number formulations described by Eqs. (13) and (14) yield very similar results. However, for plane shear, the curvature radius in Eq. (14) goes to infinity and $Ri = 0$. In the potential vortex, the shear vorticity, $\partial v_t/\partial r$, and curvature vorticity, v_t/r, just balance each other such that $Ri = 0$ again.

B. Natural Coordinate System

Equation (14) employs the tangential velocity v_t along a local streamline whose curvature is given by an inscribed circle with radius r (Fig. 5) and the respective velocity gradient, $\partial v_t/\partial r$. These quantities are calculated at every grid point, following the approach of Hirsch.[27,28] In the natural coordinate system, the magnitude of the tangential velocity corresponds to the local velocity magnitude

$$v_t = |\boldsymbol{v}| \tag{15}$$

The magnitude of the curvature radius is calculated according to

$$r = |\boldsymbol{v}^2|\big/|\boldsymbol{a}_n| \tag{16}$$

where the acceleration in the direction of the curvature radius follows from

$$\boldsymbol{a}_n = \boldsymbol{a} - \boldsymbol{v}(\boldsymbol{a}\cdot\boldsymbol{v})/|\boldsymbol{v}^2| \tag{17}$$

with the advective acceleration vector

$$\boldsymbol{a} = (\boldsymbol{v}\cdot\nabla)\boldsymbol{v} \tag{18}$$

Finally, the velocity gradient in the direction of the curvature radius

$$\frac{\partial v_t}{\partial r} = (\boldsymbol{e}_n\cdot\nabla)\boldsymbol{v} \tag{19}$$

is determined based on the unit vector pointing in the direction of the curvature radius

$$\boldsymbol{e}_n = \boldsymbol{a}_n/|\boldsymbol{a}_n| \tag{20}$$

The velocity gradient tensor, the deformation tensor, and Eqs. (15–20) are calculated in LESTUF within one loop, such that NaCoo increases the numerical effort by only 5%.

C. Implementation

Shen et al.[15] implement the Richardson number by modifying the SGS viscosity according to

$$\nu_{SGS} = \nu_{SGS,stand}(1 - \alpha Ri)^{0.5} \tag{21}$$

where α is a constant to adjust the impact of the curvature correction. NaCoo is implemented following Boysan (see Ref. 1) according to

$$\nu_{SGS} = \nu_{SGS,stand}[1/(1 + \alpha Ri)] \tag{22}$$

Boysan suggested this type of implementation for a source term modification in the dissipation equation of the k–ϵ turbulence model.

The effects of the different Richardson number formulations and their implementations are shown in Fig. 6. In both cases, the corrections substantially reduce ν_{SGS} in the vortex core region compared to the unmodified Smagorinsky approach. With NaCoo, ν_{SGS} smoothly goes to small values when approaching the vortex center, whereas the Shen et al. approach [Eqs. (13) and (21)] gives a relatively abrupt transition to zero at $r/r_c \approx 1.2$. The observed differences of the SGS viscosity profiles can be attributed primarily to the different types of implementation. We prefer the smooth transition for the sake of physical plausibility (maximum stability reached in vortex center) and numerical stability. Formulations (21) and (22) also allow for intensified momentum transport in unstable situations with $Ri < 0$.

D. Galilei Invariance

Galilei invariance, the independence of a physical model from translational motions, serves as the criterion for the universality of turbulence models. For many applications, like the ones addressed here, the violation of the concept of Galilei invariance poses no serious limitations because the applications are naturally defined in an inertial frame of reference. Nevertheless, note that approaches based on streamline curvature in general do not obey Galilei invariance.

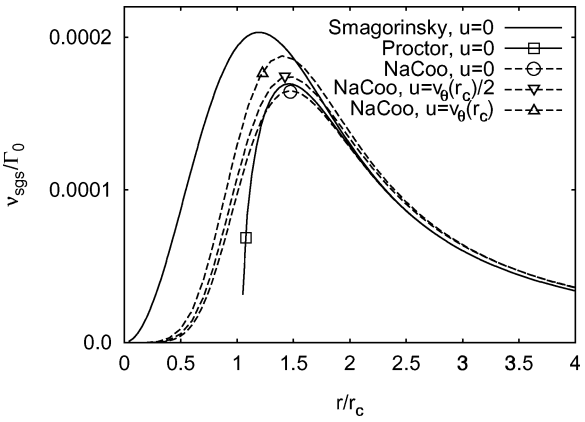

Fig. 6 Radial profiles of normalized eddy viscosity for Smagorinsky closure and modifications with $\alpha = 1$ and $r_c = 4\Delta$; NaCoo is also applied for two different levels of superimposed constant axial velocities.

Superimposition, for example, of a constant axial velocity on a vortex in a fixed frame of reference, will transform closed axisymmetric streamlines into helical streamlines with increased curvature radii and, thus, modified values of the Richardson number. An inspection of the Richardson number in Eq. (14) shows that the deformation tensor and $\partial v_t/\partial r$ remain unchanged by the superimposed axial flow. (Note that $\partial v_t/\partial r$ is not susceptible to axial flows because the direction of the curvature radius is invariant.) The magnitude of the curvature radius and the tangential velocity, however, are modified. For example, in a quite strong axial flow, where the axial velocity corresponds to the maximum circumferential velocity, the curvature radius at r_c is increased by a factor of two, whereas the tangential velocity increases only by a factor of $\sqrt{2}$. Consequently, $Ri(r_c)$ achieves a value of 0.5 instead of 1.

Figure 6 shows the respective effects on the SGS viscosity distributions for two different levels of constant superimposed axial flows. With increasing axial velocities, the effects of NaCoo are increasingly reduced. On larger radii, the decreased curvature vorticity, v_t/r, cannot fully balance the unmodified shear vorticity, $\partial v_t/\partial r$, such that the SGS viscosity increases slightly in that area. This increase reaches a maximum of less than 6% in the case of $u = v_\theta(r_c)$ and decreases again for higher axial velocities. A pragmatic way to avoid this small overestimation is to limit Ri to positive values at the expense that the intensified SGS momentum transport in unstable situations with $Ri < 0$ is suppressed.

VI. Applications

A. Single Vortices

To illustrate the effects of the streamline curvature corrections, LES of the evolution of single Lamb–Oseen vortices with $\Gamma_0 = 565$ m^2/s and $r_{c0} = 4$ m resolved by four grid points were performed. Figure 7 shows cross sections of axial vorticity for vortices with an initially superimposed random perturbation field according to case b (Sec. III) at times of $t = 0$ s and $t = 20$ s. With NaCoo, the peak vorticity of the initialized Lamb–Oseen vortex is well preserved and turbulence is damped to a reasonable level. In contrast, the high levels of SGS viscosity predicted by the standard Smagorinsky closure strongly damp both mean and fluctuating vorticity such that turbulent fluctuations become almost indiscernible.

Figure 8a compares the radial tangential velocity profiles that have developed from initialized Lamb–Oseen vortices at $t = 20$ s. With the unmodified Smagorinsky model the almost 20% reduction in maximum velocity is situated on an increased radius of $1.29r_{c0}$. Maximum velocities are also reduced with both corrections, but in the rigid-body vortex region the velocity profiles are almost conserved (preservation of peak vorticity) due to the suppressed SGS viscosity. As a consequence, the shapes of the resulting velocity profiles deviate substantially from the initiated Lamb–Oseen vortices. In the radii range between maximum velocity and potential vortex, an outer vortex core is formed that can be characterized by r^C with C between -0.35 and -0.5.

At $t = 80$ s, the velocity profile achieved with NaCoo approximates properties of the Rosenhead vortex (often also referred to as

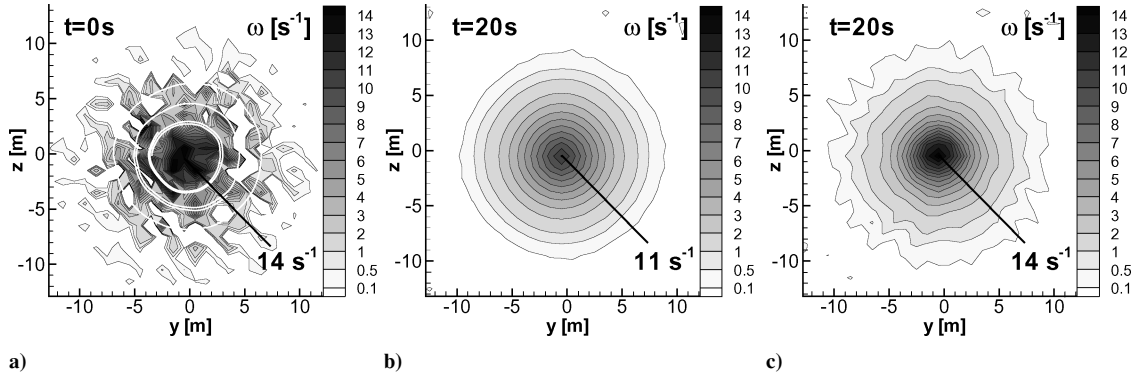

Fig. 7 Vorticity distribution of a Lamb–Oseen vortex with initially superimposed random perturbations at a) $t = 0$ s with white streamlines, b) $t = 20$ s applying the standard Smagorinsky closure, and c) $t = 20$ s applying NaCoo with $r_c = 4\Delta$ and $\alpha = 2$.

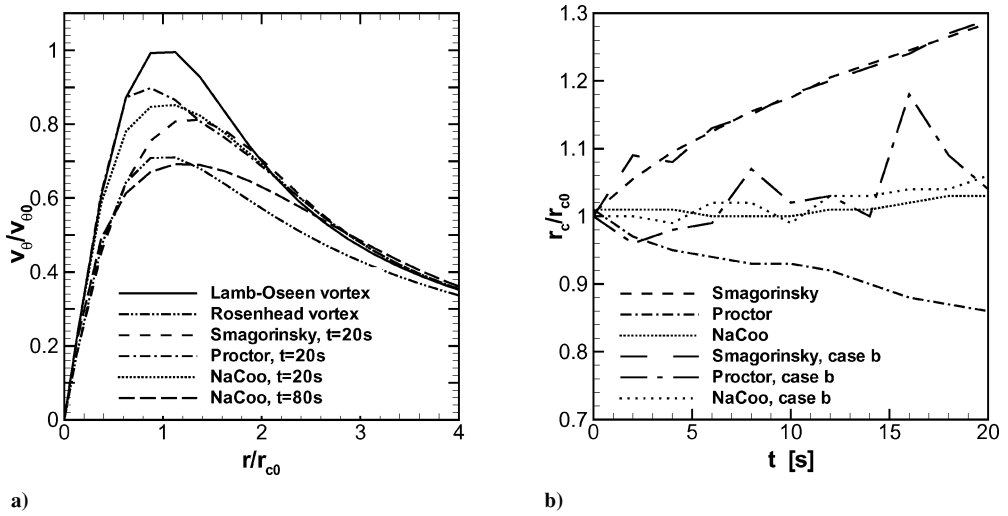

a) b)

Fig. 8 Comparison of vortex evolution employing the Smagorinsky closure and modifications with $r_c = 4\Delta$ and $\alpha = 2$: a) radial profiles of tangential velocity at different times and b) temporal evolution of core radii.

the Hallock–Burnham vortex). The Rosenhead vortex corresponds roughly to wake vortex profiles deduced from lidar field measurement data and wind-tunnel data.[29]

Figure 8b delineates the temporal evolution of vortex core radii with and without initially superimposed random perturbations. Core radii are determined as the mean distance between the vortex center and the maximum of the tangential velocity where the mean distance is an average over four individual distances calculated in four different directions, respectively. The unrealistically large growth rates with the unmodified Smagorinsky closure are not affected by turbulence. In the undisturbed vortex, Proctor's correction (see Ref. 15) even causes shrinking core radii because the region around the velocity maximum experiences diffusion only from larger radii (Fig. 6), such that the velocity maximum is shifted toward the rigid-body vortex (Fig. 8a). The disadvantage of the vorticity-based Richardson number formulation (13) becomes visible in the turbulent case: Without the normally used discrimination procedure that identifies vorticity of coherent rotation, turbulent vorticity patches receive no damping, even outside the stable core region, as is reflected in the unsteady evolution of core radii. In contrast, NaCoo, which generates reasonable small core growth rates, is not affected by the initialized spotty structure of vorticity because it is controlled by streamline curvature that is only marginally distorted by the superimposed random perturbations (Fig. 7a).

B. Aircraft Wake Vortices

Figure 9 compares the evolution of key parameters of a pair of turbulent counter-rotating wake vortices in a quiescent (case b) and a turbulent (case a) environment with and without NaCoo. The LES without the curvature correction are described in detail in Ref. 22.

As in the preceding single vortex simulations, vortex growth rate is substantially reduced with NaCoo but is not affected by different turbulence initializations until the initiation of a phase of rapid vortex decay. When fully turbulent vortices have developed for case a at $t^* = 3$ and for case b at $t^* = 6.5$ (Fig. 10 shows respective turbulence structure) the definition of a core radius holds only in a statistical sense and the evaluated average core radii start to grow rapidly. This instant coincides with the onset of rapid circulation decay, where circulation is determined as an average over radii intervals ranging from 5 to 15 m. In the initial phase of moderate decay, the diffusion phase, NaCoo reduces the decay rate as expected. In the subsequent rapid decay phase, however, the decay rate of case b with NaCoo is even increased because the initialized turbulence is less suppressed (Fig. 7). As expected, the descent rate is not modified by the curvature correction. The descent speed is mutually induced by each vortex at the center of its respective neighboring vortex and, due to the large vortex separation of almost 12 initial core

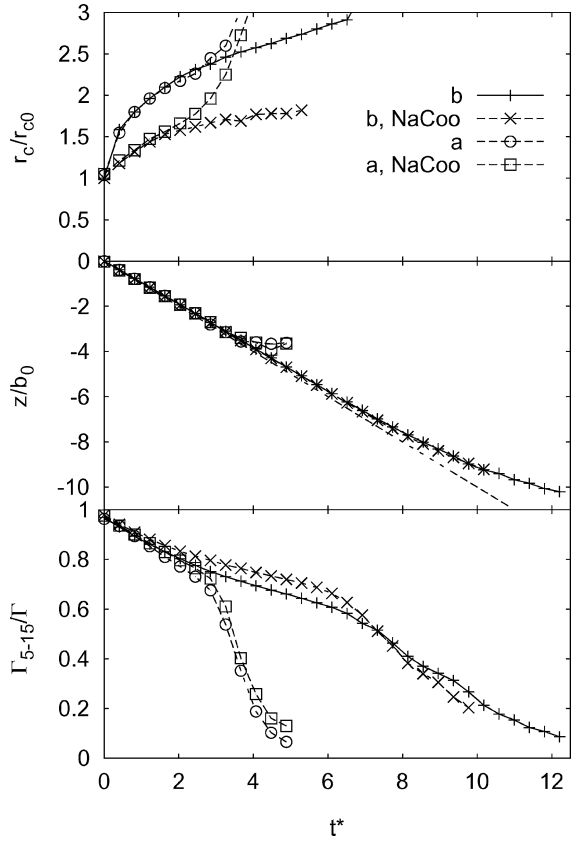

Fig. 9 Evolution of normalized vortex core radius, descent rate, and 5–15 m averaged circulation for turbulent wake vortex pairs of a B747 aircraft in quiescent (case b) and turbulent (case a) environment. NaCoo employed with $r_c = 1.7\Delta$ and $\alpha = 2$.

radii, these velocities reside in the potential vortex region of the respective neighboring vortex where $Ri \approx 0$.

Because of the major difficulties connected with measurements in the core of high-Reynolds-number wake vortices, very little experimental data for vortex core sizes and growth rates are available. Recent evaluations of three different experimental approaches suggest that minimum wake vortex core radii may be on the order of 1% of the wingspan of the aircraft.[30] Unfortunately, an adequate numerical resolution of such tight vortices is hardly feasible; we employ a ratio of $r_c/B = 8.5\%$ that, nevertheless, allows for an adequate

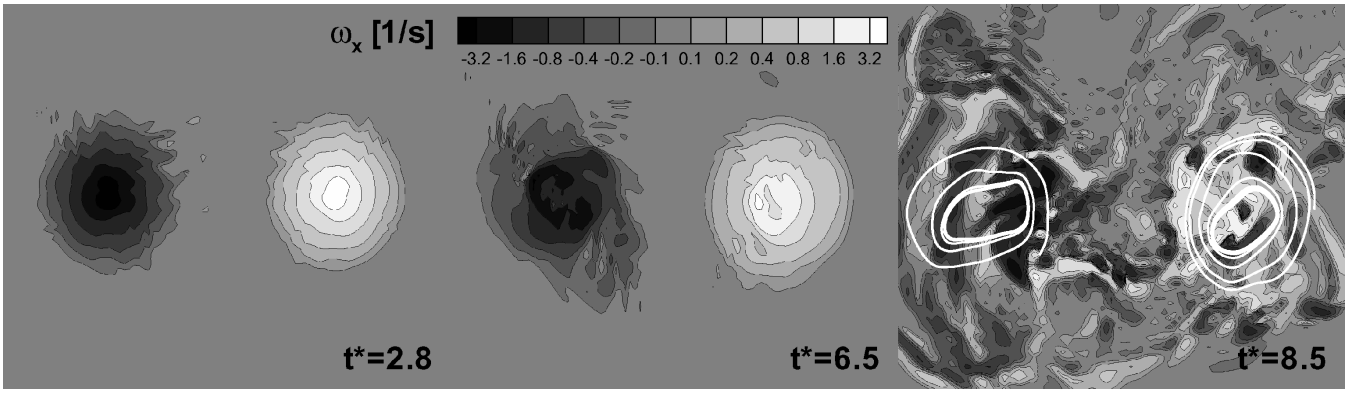

Fig. 10 Vertical–lateral cross sections of axial vorticity distribution of wake vortices initialized with aircraft-induced turbulence in a quiescent atmosphere employing NaCoo with $r_c = 1.7\Delta$ and $\alpha = 2$.

representation of main properties of wake vortices.[6] Reference 30 finds, furthermore, that the vortex cores of aircraft with retracted flaps grow roughly less than a factor of two before the onset of instability mechanisms. This corresponds well with our simulation results with NaCoo. In confined strongly swirling flows, vortex core growth rates can be close to zero.[31] In view of the minor duration of such technical flows, NaCoo should well be able to capture such constancy.

Figure 10 shows the evolution of the flow topology in vertical–lateral cross sections of the wake vortices for case b. Note that, already at $t^* = 4$, maximum axial velocities attain the same magnitude as the maximum swirl velocity components. In spite of the lack of Galilei invariance, this causes no apparent consequences for wake vortex evolution (Fig. 9). The seemingly fully incoherent flow structure at $t^* = 8.5$ represents vortices that still exhibit one-third of their initial circulation (Fig. 9) and a descent speed reduced by only 23%. It is only the white streamlines that elucidate the lingering coherence of the vortex motion. The smooth streamlines show the qualification of our current approach to determine the Richardson number based on local streamline curvature even in complex and fully turbulent situations of coherent rotation. Recent particle image velocimetry measurements[32] corroborate that the shown complex flow topologies are typical for wake vortices at high Reynolds numbers.

VII. Sensitivity

In this section, the relation of SGS viscosity-driven vortex core radius growth to the numerical resolution of the vortex, its circulation, and the curvature correction is investigated. For the decaying potential vortex, core radius growth can be described by[33]

$$r_c/r_{c0} \sim \sqrt{\nu t / r_{c0}^2} \tag{23}$$

The Smagorinsky eddy viscosity [Eq. (7)] at the core radius amounts to

$$\nu_{\mathrm{SGS}}(r_c) = \left[(c_S\Delta)^2 / \pi r_c^2\right] 0.358\Gamma_0 \tag{24}$$

The simplifying assumption, that in the LES the core radius growth can be characterized by Eq. (23) employing the value of the SGS viscosity at the instantaneous core radius [Eq. (24)], yields an analytical expression of core radius growth as a function of the numerical resolution of the initial vortex core and its circulation:

$$\frac{r_c}{r_{c0}} = \left[1 + C\,\frac{0.114(c_S\Delta)^2\Gamma_0 t}{(1+\alpha) r_{c0}^4}\right]^{\frac{1}{4}} \tag{25}$$

In Eq. (25), the effect of NaCoo is considered by the factor $(1+\alpha)$ in the denominator. This factor results from the implementation of NaCoo via a modified SGS viscosity according to Eq. (22) and $Ri(r = r_c) = 1$. Equation (25) indicates that, in the longer term, SGS viscosity causes vortex core radii growth proportional to $t^{1/4}$. The

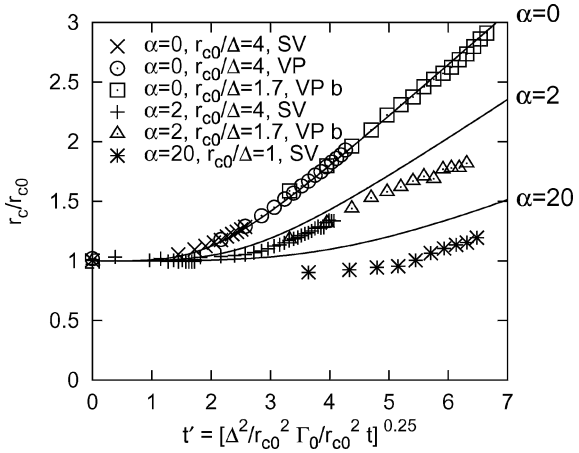

Fig. 11 Evolution of normalized core radii against normalized time; ——, parameterization according to Eq. (25) and $C = 12$.

$t^{1/4}$ dependency arises from the fact that the SGS viscosity is not a constant fluid property but, in turn, depends on Δ^2/r_c^2.

Figure 11 delineates vortex core evolution vs time according to Eq. (25) (solid lines) and different LES results (symbols) where time is normalized according to $t' = (\Delta^2/r_{c0}^2\ \Gamma_0/r_{c0}^2 t)^{1/4}$. Vortex core radii evolve along two tangents with a continuous transition in between. Depending on the constant α, the vortex core remains constant during a time span of one to three time units. This means, for example, that, according to Eq. (25), a vortex with $r_{c0}/\Delta = 10$, $\Gamma_0/r_{c0}^2 = 10\ \mathrm{s}^{-1}$, and $\alpha = 2$, would grow only for 4.6% during a period of $t' = 2$ or $t = 160$ s. Without NaCoo, the same parameter combinations would cause an increase in core radii by 12.4%. At later times vortex cores grow proportional to $t^{1/4}$ where the slope can be adjusted by α.

In Fig. 11, symbols denote simulation results of single vortices (SV) and vortex pairs (VP) with different resolutions of the core radii with and without superimposed turbulence. Without NaCoo ($\alpha = 0$), vortex growth is described consistently by Eq. (25) with $C = 12$. With the curvature correction, vortex growth is somewhat overestimated by the analytical description. The deviation of the analytical curve from simulation results is probably mainly caused by the simplifications used to derive Eq. (25). In particular, the assumption that $\nu_{\mathrm{SGS}}(r_c)$ may represent some global ν in Eq. (23) is less appropriate because, with NaCoo, the SGS viscosity exhibits a strong gradient in the vicinity of r_c (Fig. 6).

Figure 11 indicates further that, at later times, vortex growth is somewhat delayed for case b with $\alpha = 2$. A much weaker delay also seems to be present for case b and $\alpha = 0$. This is possibly caused by a redistribution of angular momentum driven by the resolved turbulence in the vortices shown in Fig. 10. The inviscid, large-scale fluctuations conserve to first order the angular momentum that

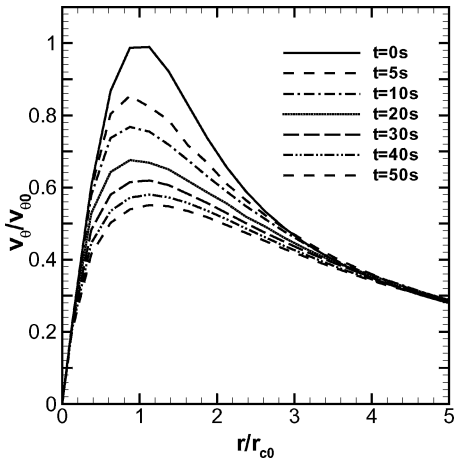

Fig. 12 Tangential velocity profiles for $\alpha = 20$ and $r_c/\Delta = 1$ at different times.

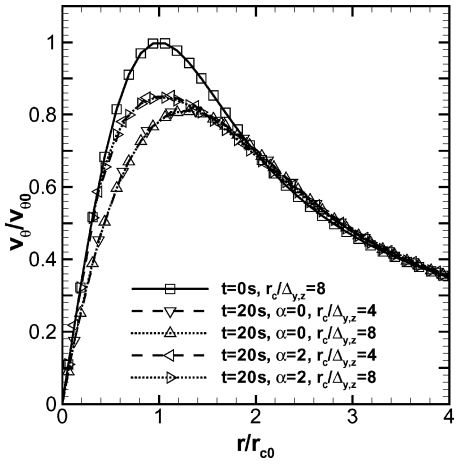

Fig. 13 Tangential velocity profiles for $r_c/\Delta = 4$ and different numerical resolutions in vortex plane with and without NaCoo; initialized profile and profiles at $t = 20$ s.

sustains the potential vortex flow and may compensate to a certain extent for the core growth caused by the SGS model.

To discuss the trends for very high values of α, one simulation is performed with $\alpha = 20$ (Fig. 12). Now vortex core growth is suppressed for a significant period of time. Intially, vortex cores even tend to shrink. Because SGS viscosity achieves larger values only on larger radii, angular momentum is sucked from larger radii without supply from smaller radii. This unequal angular momentum transport initially shifts the tangential velocity maximum along the rigid-body vortex toward smaller radii (Fig. 12). Later the vortex grows more rapidly.

To avoid indistinguishable superimposed effects of numerical resolution requirements on vortex growth, core radii were always resolved by four grid points. Different values for r_{c0}/Δ were achieved by varying the resolution perpendicular to the plane of rotation and by employing the fitting formula for anisotropic meshes.[21] Nevertheless, the contribution of discretization errors was assessed by the repetition of simulations with a doubled vortex core resolution and a respective adjustment of the axial grid spacing to achieve identical values of Δ in both simulations. Notably, the tangential velocity profiles that result from the different resolutions displayed in Fig. 13 are almost identical and cannot be distinguished from each other by the naked eye. This result demonstrates grid independence at the employed level of discretization for the second-order accurate scheme.

We conclude that Eq. (25) can already be used in the design phase of the numerical simulation to adjust vortex core growth rates caused by SGS viscosity for given values of r_{c0}, Δ, and Γ_0. For our parameter combinations (Sec. VI) a value of $\alpha = 2$ appears appropriate.

VIII. Conclusions

An adjustment of SGS parameterizations to strong streamline curvature effects is proposed. Effects of SGS closures on inadequately resolved regions of coherent rotation are analyzed by application of the Smagorinsky closure approximation to Lamb–Oseen vortices. In regions where resolved fluctuations are damped due to centrifugal stability, the SGS viscosity may achieve excessive values that further damp the resolved turbulence in the vortex and its peak vorticity and, finally, lead to untimely disintegration of vortices.

The correction termed NaCoo identifies the local degree of centrifugal stability via a rotational Richardson number that is determined from local streamline curvature at every grid point. The Richardson number, in turn, is used to modify the SGS viscosity such that SGS momentum transport is increased in unstable and decreased in stable situations. The basic principle of this approach is applicable to any other eddy-viscosity closure model. The Richardson number rests on the formulation devised by Bradshaw.[24] His Richardson number employs a plane shear squared in the denominator and, thus, assumes erroneously maximum stability at the core radius of a vortex. Here, instead the deformation tensor is used whereby a proper distribution of stability with a maximum in the center of the vortex is attained.

Features of NaCoo are discussed in comparison with other approaches from literature. The capability to resolve the slightest local streamline curvature, the balanced weighting of the correction by the type of its implementation, and the minor additional numerical effort of only 5% constitute beneficial properties of NaCoo. Main benefits of NaCoo are 1) conservation of the peak vorticity in the vortex cores, 2) reduction of vortex core radius growth rates, 3) an approach to properties of tangential velocity profiles found in experiments, 4) allowance for appropriate turbulence levels in the vicinity of the vortices, and 5) nonsuppression of vortex core meandering. These features, which corroborate results of experimental studies of turbulent vortices[29–32] denote a significant step toward a more physical modeling of inadequately resolved vortices by LES.

Applications of NaCoo to single vortices and to aircraft wake vortices in a quiescent and turbulent environment illustrate the performance of the streamline curvature correction. In particular, it is shown that streamline curvature constitutes a robust criterion for coherent rotation, even in fully turbulent and apparently incoherent flow topologies. A relation is derived that allows for the selective adjustment of vortex growth rates caused by SGS viscosity, depending on the numerical resolution of the vortex and its circulation. The relation, which indicates that vortex cores grow according to $t^{1/4}$ after a transient constancy, is corroborated by different applications.

For wake vortices, the turbulence structure within the vortices becomes more realistic and resembles flow topologies found in high-Reynolds-number laboratory experiments.[32] Vortex core growth rates can be substantially reduced to growth rates found in vortex cores of aircraft with retracted flaps.[30] Nevertheless, global parameters like wake vortex transport and decay are little affected by the correction because well-resolved secondary vorticity structures control vortex evolution.[6]

Acknowledgments

The scientific perceptions and the fruitful discussions that the author shared with Christoph Hirsch during their common stay at the Engler–Bunte Institute of the University of Karlsruhe established the basis for the current manuscript. The instrumental support during implementation and assessment of NaCoo by Thomas Gerz is greatly acknowledged. The feedback received from Robert Baumann and Robert E. Robins concerning their experiences with applications of NaCoo is appreciated.

References

[1]Sloan, D. G., Smith, P. J., and Smoot, L. D., "Modeling of Swirl in Turbulent Flow Systems," *Progress in Energy and Combustion Science*, Vol. 12, No. 3, 1986, pp. 163–250.

[2]Fu, S., and Qian, W. Q., "Development of Curvature Sensitive Nonlinear Eddy-Viscosity Model," *AIAA Journal*, Vol. 40, No. 11, 2002, pp. 2225–2233.

[3]Jakirlić, S., Hanjalić, K., and Tropea, C., "Modeling Rotating and Swirling Turbulent Flows: A Perpetual Challenge," *AIAA Journal*, Vol. 40, No. 10, 2002, pp. 1984–1996.

[4]Weber, R., Visser, B. M., and Boysan, F., "Assessment of Turbulence Modeling for Engineering Prediction of Swirling Vortices in the Near Burner Zone," *International Journal of Heat and Fluid Flow*, Vol. 11, No. 3, 1990, pp. 225–235.

[5]Sreedhar, M., and Ragab, S., "Large Eddy Simulation of Longitudinal Stationary Vortices," *Physics of Fluids*, Vol. 6, No. 7, 1994, pp. 2501–2514.

[6]Holzäpfel, F., Hofbauer, T., Darracq, D., Moet, H., Garnier, F., and Ferreira Gago, C., "Analysis of Wake Vortex Decay Mechanisms in the Atmosphere," *Aerospace Science and Technology*, Vol. 7, No. 4, 2003, pp. 263–275.

[7]Pierce, C. D., and Moin, P., "Large Eddy Simulation of a Confined Coaxial Jet with Swirl and Heat Release," AIAA Paper 98-2892, June 1998.

[8]Fan, M., Wenren, Y., Dietz, W., Xiao, M., and Steinhoff, J., "Computing Blunt Body Flows on Coarse Grids Using Vorticity Confinement," *Journal of Fluids Engineering*, Vol. 124, No. 4, 2002, pp. 876–885.

[9]Costes, M., and Kowani, G., "An Automatic Anti-Diffusion Method for Vortical Flows Based on Vorticity Confinement," *Aerospace Science and Technology*, Vol. 7, No. 1, 2003, pp. 11–21.

[10]Holzäpfel, F., Gerz, T., Frech, M., and Dörnbrack, A., "Wake Vortices in a Convective Boundary Layer and Their Influence on Following Aircraft," *Journal of Aircraft*, Vol. 37, No. 6, 2000, pp. 1001–1007.

[11]Germano, M., Piomelli, U., Moin, P., and Cabot, W. H., "A Dynamic Subgrid-Scale Eddy Viscosity Model," *Physics of Fluids A*, Vol. 3, No. 7, 1991, pp. 1760–1765.

[12]Meneveau, C., Lund, T. S., and Cabot, W. H., "A Lagrangian Dynamic Subgrid-Scale Model of Turbulence," *Journal of Fluid Mechanics*, Vol. 319, 1996, pp. 353–385.

[13]Holzäpfel, F., Hofbauer, T., Gerz, T., and Schumann, U., "Aircraft Wake Vortex Evolution and Decay in Idealized and Real Environments: Methodologies, Benefits and Limitations," *Advances in LES of Complex Flows*, edited by R. Friedrich, and W. Rodi, Vol. 65, Fluid Mechanics and Its Applications, Kluwer Academic, Dordrecht, The Netherlands, 2002, pp. 293–309.

[14]Spalart, P. R., and Shur, M., "On the Sensitization of Turbulence Models to Rotation and Curvature," *Aerospace Science and Technology*, Vol. 1, No. 5, 1997, pp. 297–302.

[15]Shen, S., Ding, F., Han, J., Lin, Y.-L., Arya, S. P., and Proctor, F. H., "Numerical Modeling Studies of Wake Vortices: Real Case Simulations," AIAA Paper 99-0755, Jan. 1999.

[16]Lewellen, D. C., Lewellen, W. S., and Xia, J., "The Influence of a Local Swirl Ratio on Tornado Intensification near the Surface," *Journal of the Atmospheric Sciences*, Vol. 57, No. 4, 2000, pp. 527–544.

[17]Gerz, T., Baumann, R., and Holzäpfel, F., "Parametric LES Studies of Far-Field Wakes Shed by Large Aircraft," Inst. of Atmospheric Physics, C-Wake Rept. TR2.2.2-1, Oberpfaffenhofen, Germany, 2003.

[18]Kaltenbach, H.-J., Gerz, T., and Schumann, U., "Large-Eddy Simulation of Homogeneous Turbulence and Diffusion in Stably Stratified Shear Flow," *Journal of Fluid Mechanics*, Vol. 280, 1994, pp. 1–40.

[19]Deardorff, J. W., "A Numerical Study of Three-Dimensional Turbulent Channel Flow at Large Reynolds Numbers," *Journal of Fluid Mechanics*, Vol. 41, 1970, pp. 453–480.

[20]Smagorinsky, J., "General Circulation Experiments with the Primitive Equations: I. The Basic Experiment," *Monthly Weather Review*, Vol. 91, No. 3, 1963, pp. 99–164.

[21]Scotti, A., Meneveau, C., and Lilly, D. K., "Generalized Smagorinsky Model for Anisotropic Grids," *Physics of Fluids A*, Vol. 5, No. 9, 1993, pp. 2306–2308.

[22]Holzäpfel, F., Gerz, T., and Baumann, R., "The Turbulent Decay of Trailing Vortex Pairs in Stably Stratified Environments," *Aerospace Science and Technology*, Vol. 5, No. 2, 2001, pp. 95–108.

[23]Lord Rayleigh, O. M., "On the Dynamics of Revolving Fluids," *Proceedings of the Royal Society of London, Series A: Mathematical an Physical Sciences*, Vol. 93, 1917, pp. 148–154.

[24]Bradshaw, P., "The Analogy Between Streamline Curvature and Buoyancy in Turbulent Shear Flow," *Journal of Fluid Mechanics*, Vol. 36, 1969, pp. 177–191.

[25]Cotel, A. J., and Breidenthal, R. E., "Turbulence Inside a Vortex," *Physics of Fluids*, Vol. 11, No. 10, 1999, pp. 3026–3029.

[26]Cotel, A. J., "Turbulence Inside a Vortex: Take Two," *Physics of Fluids*, Vol. 14, No. 8, 2002, pp. 2933–2934.

[27]Hirsch, C., "Ein Beitrag zur Wechselwirkung von Turbulenz und Drall," Ph.D. Dissertation, Lehrstuhl für Feuerungstechnik, Faculty of Chemical Engineering, Univ. of Karlsruhe, Karlsruhe, Germany, July 1995.

[28]Hirsch, C., and Leuckel, W., "A Curvature Correction for the k–ϵ Model in Engineering Applications," *Engineering Turbulence Modelling and Experiments 3: Proceedings of the Third International Symposium*, Elsevier, New York, 1996, pp. 71–80.

[29]Gerz, T., Holzäpfel, F., and Darracq, D., "Commercial Aircraft Wake Vortices," *Progress in Aerospace Sciences*, Vol. 38, No. 3, 2002, pp. 181–208.

[30]Delisi, D. P., Greene, G. C., Robins, R. E., Vicroy, D. C., and Wang, F. Y, "Aircraft Wake Vortex Core Size Measurements," AIAA Paper 2003-3811, June 2003.

[31]Holzäpfel, F., Lenze, B., and Leuckel, W., "Quintuple Hot-Wire Measurements of the Turbulence Structure in Confined Swirling Flows," *Journal of Fluids Engineering*, Vol. 121, No. 3, 1999, pp. 517–525.

[32]Vollmers, H., "Detection of Vortices and Quantitative Evaluation of Their Main Parameters from Experimental Velocity Data," *Measurement Science and Technology*, Vol. 12, No. 8, 2001, pp. 1199–1207.

[33]Zierep, J., *Ähnlichkeitsgesetze und Modellregeln der Strömungslehre*, Braun, Karlsruhe, Germany, 1982, Chap. 2.4.c.

R. So
Associate Editor